Carbon Resources Conversion 7 (2024) 100226

Contents lists available at ScienceDirect

Carbon Resources Conversion

journal homepage: www.keaipublishing.com/en/journals/carbon-resources-conversion

Original Article

Pyrolysis behaviour and kinetic analysis of waste polylactic acid composite reinforced with reed straw processing residue

Bo Chen [a], Sen Ma [b,c], Sachin Kumar [d], Zhitong Yao [e], Wanqi Feng [f], Jianbo Zhao [f,g], Xu Zhang [b], Di Cai [g,*], Hui Cao [b,*], Ian Watson [a]

[a] Systems, Power and Energy Research Division, James Watts School of Engineering, College of Science and Engineering, James Watt South, University of Glasgow, Glasgow G128QQ, United Kingdom
[b] College of Life Science and Technology, Beijing University of Chemical Technology, Beijing 100029, PR China
[c] College of Energy, State Key Laboratory of Physical Chemistry of Solid Surfaces, Xiamen University, Xiamen 361102, PR China
[d] Department of Energy Engineering, Centre of Excellence-Green and Efficient Energy Technology (CoE-GEET), Central University of Jharkhand, Ranchi 835205, India
[e] College of Materials Science and Environmental Engineering, Hangzhou Dianzi University, Hangzhou 310018, PR China
[f] College of Chemistry and Chemical Engineering, Tarim University, Alar, Xinjiang 843300, PR China
[g] National Energy R&D Center for Biorefinery, Beijing University of Chemical Technology, Beijing 100029, PR China

ARTICLE INFO

Keywords:
Biobased composite
Pyrolysis conversion
Synergy
Bio-oil
Reaction kinetics

ABSTRACT

The lignocellulose reinforced composites are commonly used sustainable materials with good mechanical and physical properties. Aiming to properly dispose and recover the potential value of discarded lignocellulose reinforced composites, the pyrolysis behaviour and kinetics of reed straw processing residual/polylactic acid (RSPR/PLA) composites, a typical 3D printing material, was investigated. Based on the TG-FTIR results, the synergistic effects between RSPR and PLA during the pyrolysis process were clarified. Compared with the FTIR spectra of PLA, the absorption peaks of CO and CO_2 disappear in the FTIR spectra of RSPR/PLA composite, which indicates RSPR provides additional free radicals for the free radical reaction of PLA, and further promoting the decomposition. The apparent activation energy of the RSPR/PLA composite pyrolysis was calculated by two *iso*-conversional methods including Flynn-Wall-Ozawa (FWO) and Kissinger-Akahira-Sunose (KAS). The average E_a of the RSPR/PLA composite (122.6 kJ mol^{-1} (FWO) and 117.9 kJ mol^{-1} (KAS)) was lower than that of solo pyrolysis of RSPR (138.5 kJ mol^{-1} (FWO) and 135.4 kJ mol^{-1} (KAS)) and the pure PLA (197.0 kJ mol^{-1} (FWO) and 196.6 kJ mol^{-1} (KAS)). The master plot method results suggested the pyrolysis of RSPR/PLA composite followed the one-dimensional (D1) diffusion model. This work provides an environmentally friendly strategy to effective thermo-chemical upgrading of the value of discarded lignocellulose reinforced composite material.

1. Introduction

With the growing awareness of the limitation of unsustainable petroleum resource and the environment and human health problems caused by traditional petroleum-based plastic products, the manufacturing of biodegradable polymeric materials is in the ascendant [1–3]. Polylactic acid (PLA) is a kind of fully degradable polymer with good mechanical properties [4], which has been widely used in packaging, medical application and other consumer products[5]. Nevertheless, owing to the obstacle of brittleness, poor gas and water barriers, and low heat distortion temperature, the pure PLA is seldom directly used as a functional material to replace the commonly used petroleum-based plastics, such as the polyethylene (PE) and polypropylene (PP) [2,6]. A well-proven route to solve above barriers is adding reinforcement phase such as rice straw, coconut coir fibre, and rice husk to produce composite materials [7–9]. In addition to endow better mechanical and physical properties, it was also indicated that the phenolic groups in the natural fibre reinforcement phase could obviously enhancing the ductility, UV light barrier and thermal resistance of PLA [10].

Although the lignocellulose/PLA composites are fully biodegradable materials, it always requires a long time to realize harmless disposal [11,12]. A pitfall of the rapid growing PLA market is the potential environment pollution once the amount of waste PLA-based composite exceeds the maximum capacity of municipal composting facilities [13]. In fact, the discarded PLA-based composites are a good carbon resource

* Corresponding authors.
E-mail addresses: caidibuct@163.com (D. Cai), caohui@mail.buct.edu.cn (H. Cao).

https://doi.org/10.1016/j.crcon.2024.100226
Received 21 September 2023; Received in revised form 8 January 2024; Accepted 17 January 2024
Available online 26 January 2024

to create additional values, rather than directly degrading in municipal composting facilities [14]. Compared to composting, which is less efficient and less economically valuable, one of the most practical strategies is to convert waste lignocellulose/PLA composites into more valuable chemicals such as bio-oil, pyrolytic gas and carbons by pyrolysis [13,15,16].

The pyrolysis mechanisms of the pure PLA have been investigated in previous research. Sun et al. (2022) pointed out transesterification and radical reactions are two major reactions involved in the PLA pyrolysis process. The transesterification reactions are occurred at relatively lower temperatures. During the process, CO, acetaldehyde, D,L-lactide and the cyclic polymers that similar to lactide, are generated by the back-biting reaction of carboxyl groups or hydroxyl groups on the PLA molecular chains [17]. When the pyrolysis temperature exceeds 300 °C, a series of free radical reactions occur, in which process the carbon free radicals and oxygen free radicals are generated from the cleavage of PLA molecular chains [18]. Since the stereoisomerism formed on carbon radicals, the PLA moiety is racemized, and further generate the *meso*-lactide, which product is the indicator that distinguish whether free radical reactions occur or not during the pyrolysis [15]. Zhang et al. (2022) studied the pyrolysis characteristics of 3D printed polylactic acid waste (3DP-PLAW) using thermogravimetric–Fourier infrared spectroscopy (TG-FTIR) and gas chromatography – mass spectrometry (GC–MS). They found that the main pyrolysis products of 3DP-PLAW consists of CO, CO_2, CH_4, acetaldehyde, esters (*meso*-lactide and D, L lactide), and other carbon-based compounds. Furthermore, the high volatile matter in 3DP-PLAW contributes to a more efficient thermochemical conversion.

Many studies suggest the co-pyrolysis of plastics and lignocelluloses could facilitate the pyrolysis reaction and reduce the energy consumption, which is attributed to the synergistic effect between these two distinct types of feedstocks [4,19,20]. Compared to pyrolysis, co-pyrolysis always generates homogenous stable products with low oxygen content and high caloric value [21]. Sun et al. (2019) suggested there are synergistic effect between wood flour and PLA during the co-pyrolysis process, in which process the free radical reaction of PLA can be promoted due to the presence of wood flour. In another research, Qi et al., (2018) explored the generation of aromatic hydrocarbons through the co-pyrolysis of microalgae and polypropylene (PP). The co-pyrolysis of microalgae and PP exhibits a synergistic effect, leading to a more significant production of aromatic hydrocarbons in comparison to the individual pyrolysis of microalgae and PP. For the pyrolytic recycling of the lignocelluloses/plastic composite materials, the above-mentioned statements regarding the positive effect of the natural fibers as reinforcement on the pyrolysis behavior of composites are generally applicable. For instance, Lin et al., (2019) evaluated the products distribution and synergy during the catalytic pyrolysis of wood-plastic composite (WPC). The results suggest that there were strong synergistic interactions between poplar and PP in the process of WPC pyrolysis, which promote the yield of alkenes. In addition, Sun et al., (2013) investigated the products distribution during the pyrolysis of wood-plastic composites (WPC) using pyrolysis-gas chromatography/mass spectrometry (Py-GC/MS) and reported poplar wood provided radicals to promote the breaking of polymer chains, resulting in the formation of lighter paraffins. Nonetheless, the pyrolysis behaviors of the lignocelluloses/PLA composite are rarely studied.

To gain deeper insights into the thermal properties and pyrolysis kinetics of solid materials, thermogravimetric analysis (TGA) is a widely employed method with high accuracy [22]. In the case of studying the pyrolytic kinetics of PLA-based composites, model-free methods are reliable methods which can be used for the calculation of various thermodynamic parameters, including activation energy, pre-exponential factor, and order of reaction [23]. Commonly utilized methods in previous research include the Flynn-Wall-Ozawa (FWO) method, the Starink method, and the Kissinger–Akahira–Sunose (KAS) method. [24–26].

Compared to directly employing lignocellulosic biomass as reinforcement in PLA composite production, using the solid residue from biorefinery plant can markedly enhance the economic feasibility and streamline the management of solid waste in subsequent stages [6,27]. The pyrolysis behavior of the blend of PLA and wood flour has been well studied in previous studies (Sun et al., 2021b, 2021a, 2019), and limited research investigated the pyrolysis behavior of PLA composite [28]. However, to our best knowledge, no investigation has been done on the pyrolysis behavior of biorefinery residue reinforced PLA composites. In the present work, the pyrolysis kinetics of reed straw processing residual (RSPR) reinforced polylactic acid (PLA) composite was investigated by the Flynn-Wall-Ozawa (FWO) method, the Kissinger–Akahira–Sunose (KAS) method, the Friedman method and master-plot method. During the pyrolysis of RSPR/PLA composites, the evolved gaseous products were monitored and analyzed using TG-FTIR. The primary objective of this study is to maximize the value of waste PLA-based composites in the energy area and provide basic understanding of thermo-chemical conversion manner to support the rapid growth of PLA industry.

2. Materials and methods

2.1. Materials and characteristics

2.1.1. Materials and preparation of RSPR/PLA composite

The reed straw (RS) was harvested in Changping district, Beijing, China. After drying out and milling into ~60 meshes, the RS powder was pre-treated by dilute NaOH aqueous solution, followed by collection and hydrolysis by cellulase (the pre-treatment conditions were in accordance with our previous report [29]). Then, the solid residual that defined as the RSPR was collected and was dried at 105 ℃ for 24 h. After milling, the RSPR was used as the reinforcement phase for the RSPR/PLA composite. The chemical constituents (cellulose, hemicellulose, lignin) of the RSPR were determined by the standard of National Renewable Energy Laboratory of USA [30], and the results showed the chemical constituents of RSPR are 39.15±1.2 wt% of cellulose, 22.5±0.9 wt% of hemicellulose, 19.6±0.4 wt% of lignin and 18.75±0.4 wt% of other substances, respectively. The PLA (4032D) was purchased from Natureworks LLC, USA.

A COPERION ZSK series twin-screw extruder (Werner & Pfleiderer, Germany) was used for the preparation of RSPR/PLA composites. A mixture of PLA (70 wt%), RSPR (20 wt%), and coupling agent (3 wt% synthesis of plant ester, 3 wt% PEG600 and 4 wt% KH550) was extruded under the heating zone temperatures of 145–170 ℃ with screw speed of 60 rpm. The injection of the standard specimen was prepared at 145–160 ℃ and 50 MPa by an injection moulding machine (HTF 120 X2, Haitian, China).

2.1.2. Characteristics of RSPR/PLA composite

The volatiles, moisture, fixed carbon and ash content in RSPR, PLA and RSPR/PLA composite were determined by the proximate analysis (LECO TGA701), and the ultimate analysis (CHN628, LECO, USA). The results were listed in Table 1. According to the proximate analysis results, the volatiles in RSPR (73.13 wt%), PLA (99.88 wt%) and RSPR/PLA composite (95.25 wt%) was the predominated fraction, which inferred low solid products yield in the pyrolysis process [24,25]. Meanwhile, according to the ultimate analysis results, carbon and oxygen were the main elements in all the tested specimens (93.69 wt% for RSPR, 94.22 wt% for PLA and 93.4 wt% for RSPR/PLA composite). The N element (0.4 wt%) in RSPR could be assigned to the remaining proteins during the fermentation process. While the N elements in the RSPR/PLA composite could be attributed to the introduction of couple agent in the preparation process.

2.2. Thermogravimetric and pyrolysis products analysis

Thermal decomposition behaviour of RSPR, PLA and RSPR/PLA composite were characterized using TGA/DSC3+ (Mettler,

Table 1
Ultimate analysis and proximate analysis results of the specimens.

Samples	Ultimate analysis [a] (wt%)				Proximate analysis [b] (wt%)			
	C	H	N	O *	Moisture	Volatile	Ash	Fixed carbon
RSPR	44.72±0.45	5.91±0.09	0.4±0.09	48.97±0.53	5.3±0.15	73.13±0.75	6.07±0.11	14.5±0.15
PLA	49.94±0.26	5.76±0.12	0.02±0.001	44.28±0.35	0	99.88±0.08	0.09±0.002	0.03±0.001
RSPR/PLA composite	51.96±0.23	6.3±0.14	0.3±0.01	41.44±0.15	0.76±0.02	95.25±0.66	1.55±0.02	2.44±0.07

[a] On dry and ash-free basis (wt%).
[b] On dry mass fraction basis (wt%).
* Calculated by difference.

Switzerland). The experiments were conducted from 30 ℃ to 700 ℃ at different heating rates (5 ℃ min^{-1}, 10 ℃ min^{-1} and 20 ℃ min^{-1}) in nitrogen atmosphere. The TGA experiment was conducted three times to ensure the reproducibility and trustworthiness of the data.

The gaseous products were analyzed by TG-FTIR. In this process, the RSPR, PLA and RSPR/PLA composite specimens were heating from 30 ℃ to 800 ℃, with a heating rate of 10 ℃ min^{-1}, within a purity nitrogen atmosphere flowing at a rate of 50 mL min^{-1} by using a TG 209F1 Libra thermal analyser (NETZSCH, Germany). The temperature of transfer line connecting to the TG-FTIR apparatus was maintained at 250 ℃. The identification of functional groups in the gas products was carried out using an FTIR spectrometer (Nicolet 6700, Thermo Fisher, USA) with a spectral resolution of 4 cm^{-1} in the spectral region from 4500 cm^{-1} to 500 cm^{-1}.

2.3. Kinetics analysis

To better understand the pyrolysis characteristics of the RSPR/PLA composite, we conducted a kinetic analysis to determine the pyrolysis kinetics. The kinetic equation describing the decomposition rate is expressed as follows:

$$\frac{d\alpha}{dt} = k(t)f(\alpha) \tag{1}$$

where k is the decomposition rate constant, $f(\alpha)$ represents the reaction model, t represents reaction time and α is the conversion rate, which can be described as:

$$\alpha = \frac{m_0 - m_t}{m_0 - m_f} \tag{2}$$

where m_0 is the initial weight of the specimens, m_t is weight at time t and m_f is the remaining weight at the end of the pyrolysis process. Substituting the Arrhenius equation into Eq. (1), the Eq. (1) can be described as:

$$\frac{d\alpha}{dt} = Aexp\left(\frac{-E_a}{RT}\right)f(\alpha) \tag{3}$$

where A is the pre-exponential factor (s^{-1}), E_a is the activation energy (kJ/mol). R is the universal gas constant (8.314 J K^{-1} mol^{-1}), and T is the absolute temperature (K).

For the non-isothermal TGA analysis, the heating rate β is constant which can be defined as:

$$\beta = \frac{dT}{dt} \tag{4}$$

Combining Eq.3 with Eq.4, the following equation is obtained:

$$\frac{d\alpha}{dT} = \frac{A}{\beta}exp\left(\frac{-E_a}{RT}\right)f(\alpha) \tag{5}$$

2.3.1. Model-free methods

Model-free methods do not require the knowledge of the reaction mechanism, which helps avoid errors in estimating E_a. KAS and FWO which are two integral model-free methods were employed to analyse the pyrolytic kinetics analysis of RSPR, PLA and RSPR/PLA composite. In additional, Friedman method, a differential model-free method, has been adopted to calculate the E value to reduce the error in results. The equations for these three model-free methods can be expressed as follows:

$$\text{KAS}: ln\left(\frac{\beta}{T^2}\right) = ln\frac{AR}{E_a g(\alpha)} - \frac{E_a}{RT} \tag{6}$$

$$\text{FWO}: ln(\beta) = ln\frac{0.0048AE}{Rg(\alpha)} - \frac{1.0516E_a}{RT} \tag{7}$$

$$\text{Friedman}: ln\left(\frac{d\alpha}{dt}\right) = \ln[Af(\alpha)] - \frac{E_a}{RT} \tag{8}$$

The activation energy E_a can be estimated by the slopes of the $\frac{1}{T}$ versus $ln\left(\frac{\beta}{T^2}\right)$ plots (KAS), the $\frac{1}{T}$ versus $ln(\beta)$ plots (FWO) and $ln\left(\frac{d\alpha}{dt}\right)$ versus $\frac{1}{T}$ plots (Friedman) [26,31–33].

2.3.2. Master-plot method

The Master-plot method was employed to determine the most suitable reaction mechanism model for the pyrolysis process. This method is a straightforward graphical approach, wherein experimental master plots and theoretical master plots are generated based on Eq. (9). [34].

$$\frac{g(\alpha)}{g(0.5)} = \frac{E_a AP(u_\alpha)/\beta R}{E_a AP(u_{0.5})/\beta R} = \frac{P(u_\alpha)}{P(u_{0.5})} \tag{9}$$

where the theoretical plots of $g(\alpha)/g$ (0.5) versus α were derived from different solid-state reaction models, which were summarized in Table S1. Meanwhile, the experimental plots of $P(u_\alpha)/P$ ($u_{0.5}$) versus α were calculated using the kinetic parameters obtained in section 2.4.1. The most appropriate reaction mechanism model is determined when the experimental master plot curves align with or overlap the theoretical master plot curves.

2.3.3. Thermodynamic parameters

The kinetic parameters and reaction mechanism model obtained from the model-free methods and master-plot method were utilized to compute the thermodynamic parameters of RSPR/PLA composite, including the pre-exponential factor A (s^{-1}) [35], enthalpy change ΔH (kJ/mol), Gibbs free energy ΔG (kJ/mol), and changes in entropy ΔS (kJ/mol K^{-1}). These calculations were performed using the equations below:

$$A = \frac{2\beta E_a}{RT_m\alpha_m^{-2}}\exp\left(\frac{E_a}{RT_m}\right) \tag{10}$$

$$\Delta H = E - RT \tag{11}$$

$$\Delta G = E_a + RT_m\ln(K_B T_m/hA) \tag{12}$$

$$\Delta S = (\Delta H - \Delta G)/T_m \tag{13}$$

where K_B is the Boltzmann constant (1.3819×10^{-23} J K^{-1}), h is the Planck constant (6.626×10^{-34} J s^{-1}), T_m is the DTG peak temperature

and α_m is the conversion rate at peak temperature.

3. Results and discussion

3.1. Thermogravimetric analysis

Fig. 1 showed the TGA and DTG curves of RSPR, PLA and RSPR/PLA composite at heating rate of 10 ℃ min^{-1}. The thermal decomposition curves of RSPR could be divided into three stages. The initial stage, occurring below 200 ℃, was attributed to the evaporation of the moisture and small molecule volatile substance compounds in RSPR [36]. The second stage around 200–350 ℃ was caused by the depolymerization of hemicellulose and cellulose. Because of the relatively loose structure and poor thermal stability, the temperature for hemicelluloses depolymerization (200–300 ℃) was lower than that of the crystalline regions containing cellulose (240–350 ℃) [20,37,38]. The third stage is the decomposition of lignin, it lasted until the end of pyrolysis. Since the structure of lignin is very stable and rich in aromatic subunits, the decomposition of lignin exists almost throughout the whole pyrolysis process [39].

The decomposition of the pure PLA was completed in single stage (300–398 ℃). The orderly and repetitive molecular chains within PLA resulted in a concentrated pyrolysis temperature range, leading to a narrow DTG peak [4]. By contrast, the decomposition of RSPR/PLA composites can be divided into three stages. Similar with the phenomenon of the RPSR pyrolysis, the initial stage ranges from 200 °C to 330 °C was caused by the decomposition of hemicellulose and part of cellulose, while the second stage, occurring within the range of 330 °C to 440 °C, was associated with the pyrolysis of PLA and the remaining highly crystalline cellulose. The third stage (>440 °C) was attributed to the pyrolysis of lignin and coupling agent in RSPR/PLA composites.

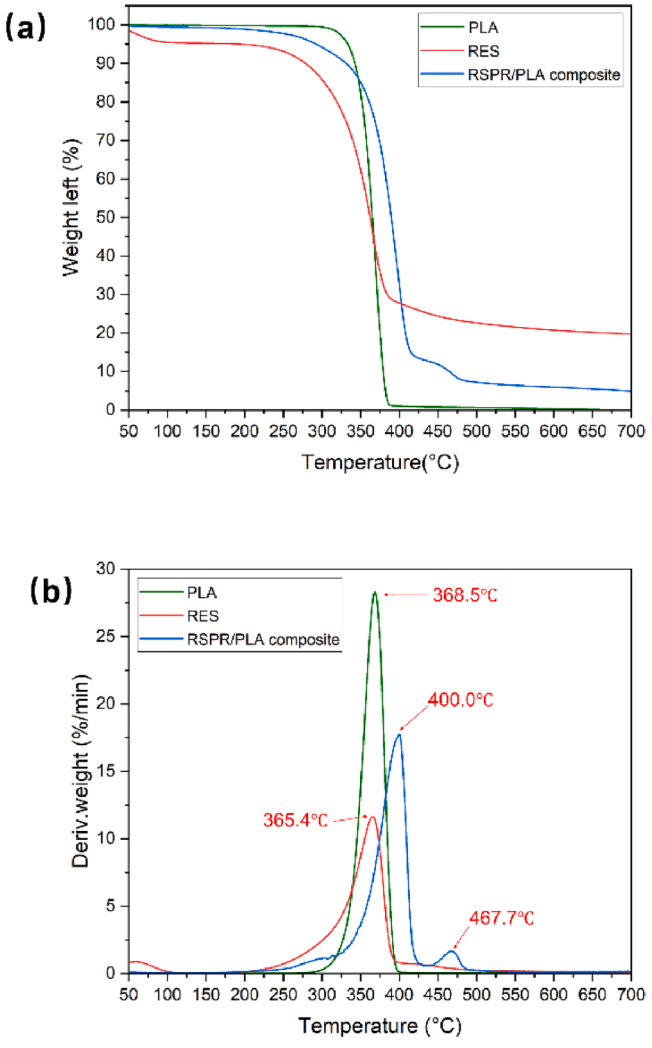

Fig. 1. (a) TGA and (b) DTG curves of RSPR, PLA and RSPR/PLA composite at heating rate of 10 ℃/min.

In comparison to the pyrolysis of RSPR and pure PLA, the DTG peak of the RSPR/PLA composites shifted to higher temperature. This phenomenon can be explained as follow: after alkali pre-treatment and enzymatic hydrolysis, the hydrogen bonds in the initial RSPS fibre was interrupted, thereby increased the roughness of the RSPR surface. Consequentially, the increased hydroxyl groups on the surface of the RSPR improved the adhesion of the reinforcement phase to the polymer matrix [40]. Furthermore, the addition of coupling agents including the synthetic plant ester, PEG600 and KH550 could also positively affect the thermal stability of the composite. With the increase of the heating rate, the peaks in all the DTG curves of the tested specimens shifted to higher temperatures, owing to the increase of the thermal hysteresis (Figs. S1-S3) [41].

3.2. Volatile products analysis by TG-FTIR

The characterization and comparison of volatile products generated during the pyrolysis of RSPR, PLA, and RSPR/PLA composite were conducted. Fig. 2(a, c and e) illustrated the 3D FTIR spectra of the gaseous products for RSPR, PLA, and the RSPR/PLA composite during the pyrolysis. According to the Beer-Lambert law, the absorbance of the gaseous pyrolysis products should be proportional to the concentration [42]. Thus, the temperature range that aligned with the peak absorption in the FTIR spectra indicated the most pyrolysis products were generated. Specifically, the highest absorption peaks for RSPR occurred within the temperature range of 320–350 °C, whereas for PLA, they were in the range of 380–420 °C. In contrast, the RSPR/PLA composite exhibited its maximum absorption peaks in the temperature range of 390–430 °C. Thus, compared to pyrolysis of RSPR and the pure PLA, the predominated pyrolysis products range shifted to higher temperatures in the group of RSPR/PLA composite. This may be due to the improved adhesion between RSPR and PLA matrix caused by the presence of coupling agents in the composite material [6].

Fig. 2(b, d and f) showed the FTIR spectrums of RSPR, PLA and RSPR/PLA composite at different pyrolysis temperature. For the FTIR spectra of RSPR/PLA composite, the bands located in the range of 4000–3500 cm^{-1} corresponded to the water released by dehydration and evaporation [43]. The peaks at the range of 3100–2640 cm^{-1} can be assigned to the stretching vibration of C-H bonds, inferring the existence of hydrocarbon [44]. Specially, the peaks located in the range of 2800–2640 cm^{-1} in FTIR spectra was the stretching vibration peak of the O = C-H group[45], which suggested the existence of aldehydes. The peaks within the range of 2400–2250 cm^{-1} were associated with the C = O stretching vibration, specifically related to CO_2, which was generated from the cracking and reforming of carbonyl and carboxyl during the pyrolysis [43]. The absorption at the range of 2240–2000 cm^{-1} was related to CO. The strong peaks located at the ranged of 1850–1600 cm^{-1} was attributed to the stretching vibration of C = O, indicating the generation of carbonyl compounds such as ester, ketone, acid, etc. [4]. The peaks in the range of 1400–1000 cm^{-1} were the stretching vibration of C-O(H), which suggests the existence of alcohols, phenols and ethers [13]. The absorption peaks of the RSPR/PLA composite were mainly located at the range of 3100–2640 cm^{-1} and 1850–1600 cm^{-1}, indicating the generation of hydrocarbons and carbonyl compounds. Therefore, the decomposition of RSPR/PLA composite mainly occurred at the methyl and ester bonds [13]. The main absorption peaks of RSPR located at the range of 4000–3500 cm^{-1}, 3100–2640 cm^{-1}, 2400–2250 cm^{-1}, 2240–2000 cm^{-1}, 1850–1600 cm^{-1} and 1400–1000 cm^{-1} corresponded to the existence of water, hydrocarbon, aldehydes, carbon

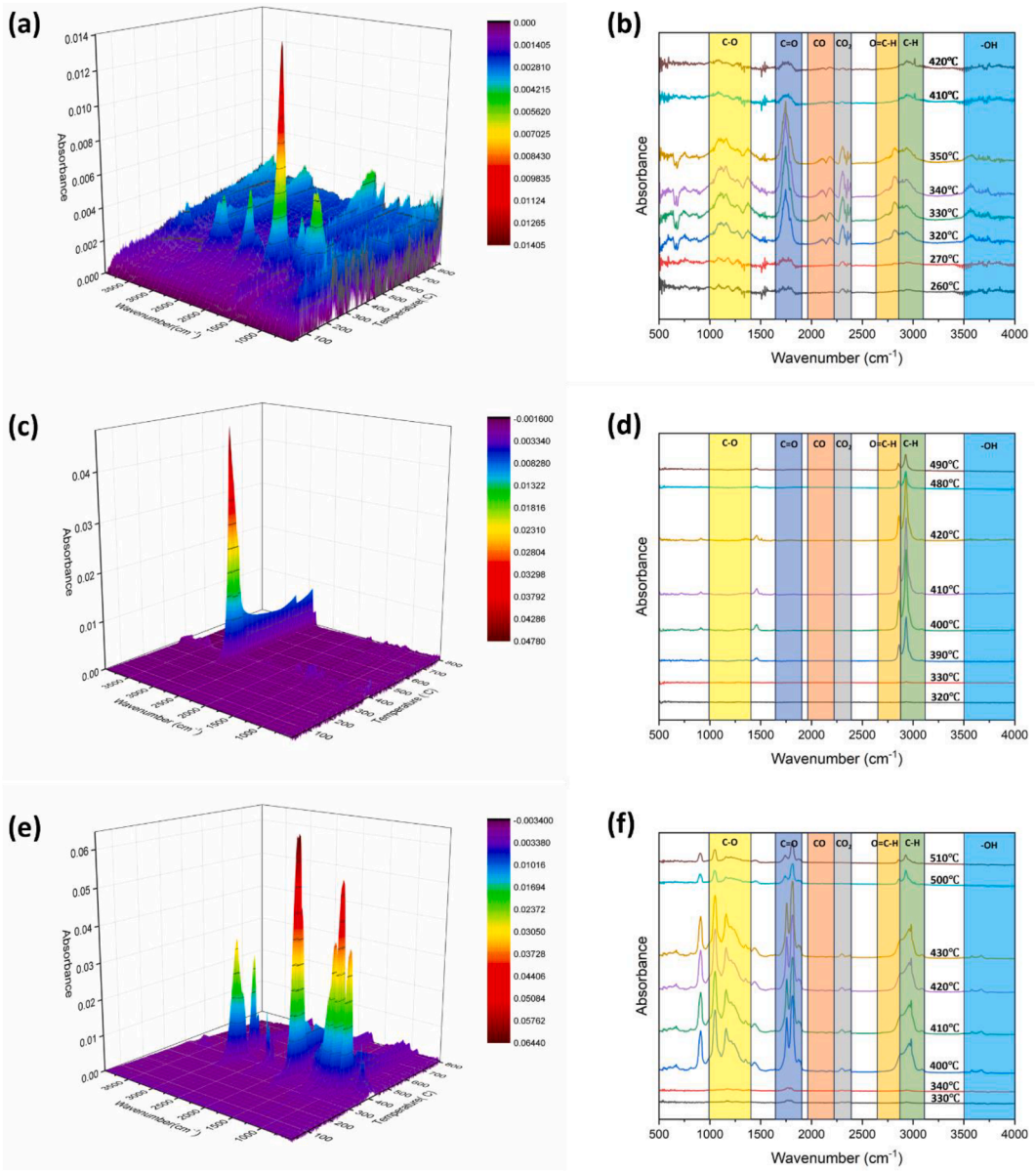

Fig. 2. 3D FTIR spectrums of (a) RSPR, (c) PLA and (e) RSPR/PLA composite; FTIR spectrum of (b) RSPR, (d) PLA and (f) RSPR/PLA composite during pyrolysis at different temperatures with heating rate of 10 ℃ min^{-1}.

dioxide, carbon monoxide, carbonyl compounds and alcohols, phenols, etc. respectively [43]. The mainly gaseous products of PLA were located at the range of 3100–2640 cm^{-1}, which were related to the presence of hydrocarbon and aldehydes.

Compared with the FTIR spectra of the gaseous products of PLA and RSPR, there was no additional absorption peak occurred in the spectra of RSPR/PLA composite, indicating there was no new product during the pyrolysis process. The largest change in FTIR spectra peaks of RSPR/PLA composite was C = O bond compared with that of PLA. This could be attributed to the presence of RSPR in composite promotes the free radical reaction of PLA, leading to the increase production of ester groups [15]. Furthermore, in comparison with the FTIR spectra of RSPR, CO group was nearly vanished, and the CO_2 group was also significantly weakened in the FTIR spectra of RSPR/PLA composite. It has been reported that CO and CO_2 were the transesterification products of PLA pyrolysis [19]. The reduction of CO and CO_2 group in the FTIR spectra of RSPR/PLA composite demonstrated the presence of RSPR in composite promoted the reaction mechanism of PLA pyrolysis from the transesterification reaction to the free radical reaction.

3.3. Kinetic analysis

3.3.1. Activation energy calculation

The pyrolysis kinetics were studied by three model-free methods. Fig. 3 showed the linear relationship between $\frac{1}{T}$ and $ln\left(\frac{\beta}{T^2}\right)$ (KAS), $\frac{1}{T}$ and $ln(\beta)$ (FWO) and $ln\left(\frac{d\alpha}{dt}\right)$ and $\frac{1}{T}$ (Friedman) at different heating rates. The activation energy (E_a) and linear correlation coefficients (R^2) of RSPR, PLA and RSPR/PLA composite at different conversion rate were calculated by KAS, FWO and Friedman methods (Table 2). The R^2 values of different specimens and kinetic methods were between 0.95 and 1, suggesting the kinetic methods was conformed with the reaction mechanism of feedstocks' pyrolysis. The E_a values of three models at different conversion rates were generally similar, indicating the models were suitable for analysing the kinetics of the RSPR/PLA composite pyrolysis. Meanwhile, FWO exhibited a better performance in calculating E than KAS and Friedman method according to the R^2 values. Table 2 shows the E value calculated by FWO method were always higher than those by KAS methods, which ascribed to the difference in

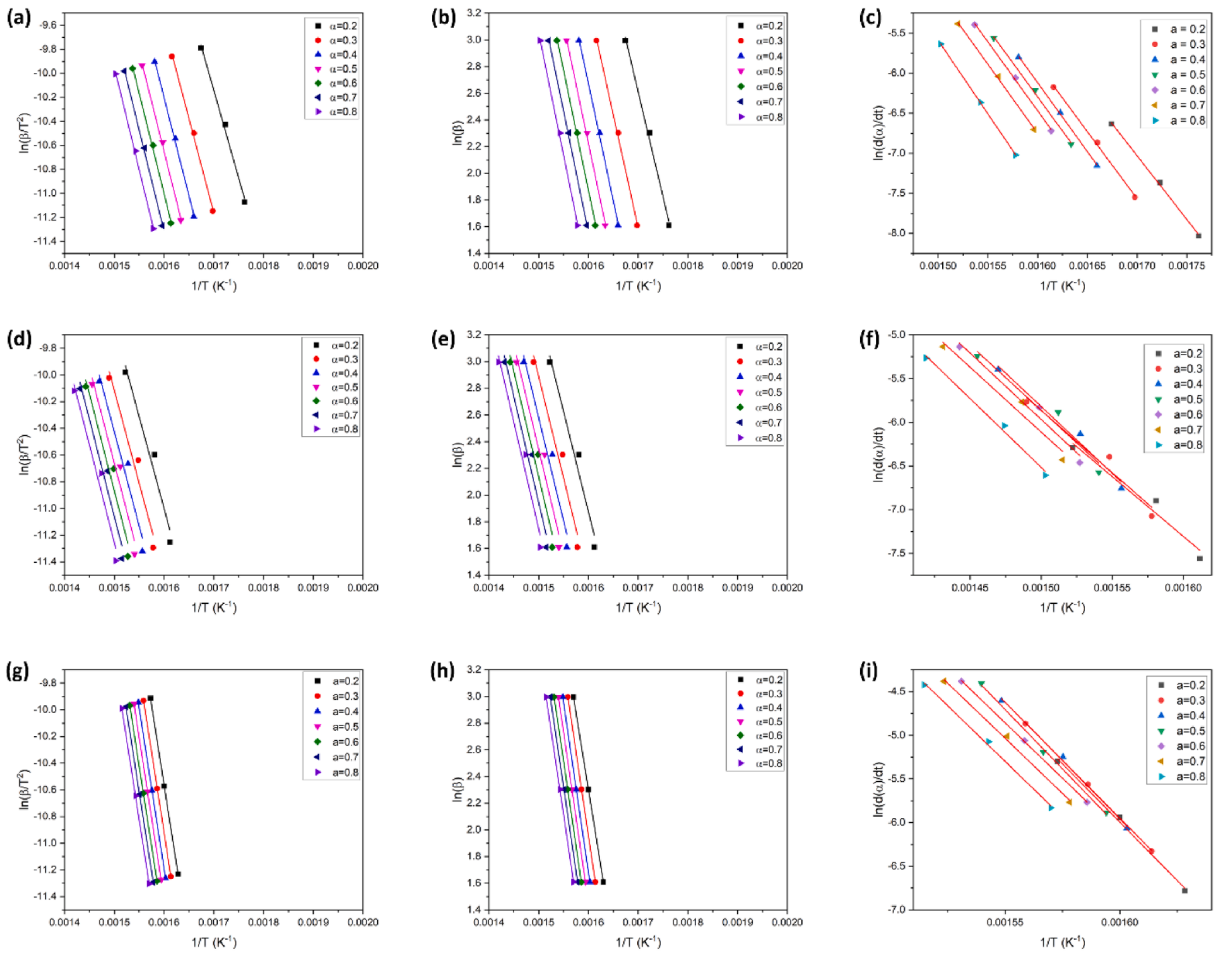

Fig. 3. Linear plots for activation energy determination by FWO method of (a) RSPR, (d) PLA, (g) RSPR/PLA composite; KAS method of (b) RSPR, (e) PLA, (h) RSPR/PLA composite; Friedman method of (c) RSPR, (f) PLA, (i) RSPR/PLA composite.

the derivation process and error range of different models [46].

E_a was the minimum energy required for a chemical reaction to be occurred [47]. A higher E_a value signifies a greater amount of energy, or an extended reaction time was required in the pyrolysis process. For the RSPR pyrolysis, the E_a increased with the increases of conversion rate (Fig. 4). The initial E_a was lower than that of PLA because the volatiles and small molecule substances from RSPR were eliminated at this stage [48]. Then, the E_a was increased at $\alpha = 0.3$. The large increase of E_a at $\alpha = 0.3$ could be attributed to the onset of decomposition of the hemicellulose and cellulose in RSPR. The steady increase of E_a after $\alpha = 0.3$ inferred the breakdown of strong chemical bond (e.g., benzene ring in lignin), which required an increasing amount of energy and initiates at higher temperatures [49]. At the end of the pyrolysis progress, the remained ash would hinder the diffusion of volatiles. Thus, the E_a reached highest value at $\alpha = 0.8$ [46].

For the pure PLA pyrolysis, the average E_a values were 197.0 kJ mol^{-1}, 196.6 kJ mol^{-1} and 217.1 kJ mol^{-1} by FWO and KAS methods, respectively. It can be observed that with the increase of the conversion rate, the E_a was first increased, followed by a stable stage, and then was slightly dropped after $\alpha = 0.5$. The PLA pyrolysis process can be divided into two reactions: transesterification and free radical reaction, transesterification reaction takes place at the beginning of PLA pyrolysis while the free radical reaction happens above 300 °C [50]. Because of the cleavage of covalent bonds. free radical reaction requires more energy when compared to the transesterification reaction [4]. So, with the increase of conversion rate, the E_a increased. Compared to the E_a value of RSPR, the E_a value of PLA is higher and more stable throughout the entire pyrolysis process. The lower E_a value of RSPR could be ascribed to the relatively high content of hemicellulose in RSPR fibre, which has a loose structure and requires less energy to decompose [37]. In addition, due to the neat and repeated structure of PLA, the E_a value of PLA is more stable than that of RSPR.

For the pyrolysis of RSPR/PLA composite, the average E_a value (121.5 kJ mol^{-1}) was lower than that of RSPR (138.5 kJ mol^{-1}) and the pure PLA (205.5 kJ mol^{-1}) groups. Therefore, the RSPR as the reinforcement phase in the composite material could significantly reduce the E_a. The E_a value during the whole pyrolysis progress of the composite was lower than that other two groups. At the physical level, energy conversion during co-pyrolysis cannot be lower than that when pyrolyzing the individual material separately. Therefore, the reason for reduction of the E_a was ascribed to the synergetic effects between RSPR reinforcement and PLA matrix [19], and the promotion of the free radical reactions of PLA by the free radical released from lignin in RSPR [51].

Meanwhile, the E_a value curve of RSPR/PLA composite was similar to that of RSPR. At the first stage, owing to the transformation of the dominate reaction from the transesterification to the free radical reaction, the energy required was higher, which further leaded to the increase of the E_a. Then, as the temperature reached the threshold for the initiation of the free radical reaction of PLA, the energy consumption was stable. However, because the cellulose, hemicellulose and lignin in RSPR started to decompose during this period ($\alpha = 0.2$–0.8), the E_a was further slowly increased.

3.3.2. *Kinetics model determination by master plot method*

Master plot method was further adopted to determine the reaction

Table 2
The activation energy and linear correlation coefficients of the pyrolysis of RSPR, PLA and RSPR/PLA at different conversion rates calculated by FWO, KAS and Friedman method.

α	RSPR						PLA						RSPR/PLA composite					
	FWO		KAS		Friedman		FWO		KAS		Friedman		FWO		KAS		Friedman	
	E_a (kJ/mol)	R^2	E_a (kJ/mol)	R^2	E_a (kJ/mol)	R^2	E_a (kJ/mol)	R^2	E_a (kJ/mol)	R^2	E_a (kJ/mol)	R^2	E_a (kJ/mol)	R^2	E_a (kJ/mol)	R^2	E_a (kJ/mol)	R^2
0.2	124.6	0.996	121.3	0.995	132.2	0.998	197.6	1.0	197.3	1.0	220.2	0.991	118.7	0.97	114.2	0.96	113.7	0.959
0.3	133.7	0.998	130.6	0.998	139.6	0.998	199.5	1.0	199.4	1.0	221.1	0.999	120.2	0.97	115.6	0.96	118.5	0.958
0.4	138.9	0.998	135.8	0.998	140.1	0.999	200.7	1.0	200.5	1.0	222.2	0.993	121.8	0.96	117.1	0.96	120.2	0.98
0.5	140.8	0.998	137.6	0.998	141.7	0.999	201.4	1.0	201.2	1.0	226	0.996	123.8	0.96	119.1	0.96	124.2	0.949
0.6	142.2	0.998	139.0	0.998	143.1	0.998	200.6	1.0	200.3	1.0	211	0.999	125.0	0.97	120.3	0.96	126.4	0.974
0.7	143.4	0.998	140.2	0.998	143.7	0.998	199.6	1.0	199.3	1.0	209.9	0.994	125.8	0.97	121.1	0.96	128.2	0.962
0.8	145.3	0.998	142.0	0.999	152.8	1	198.9	1.0	198.4	1.0	209.1	0.994	126.4	0.97	121.6	0.96	130.8	0.992
Average	138.4	–	135.2	–	141.9	–	199.8	–	199.5	–	217.1	–	123.1	–	118.4	–	123.1	–

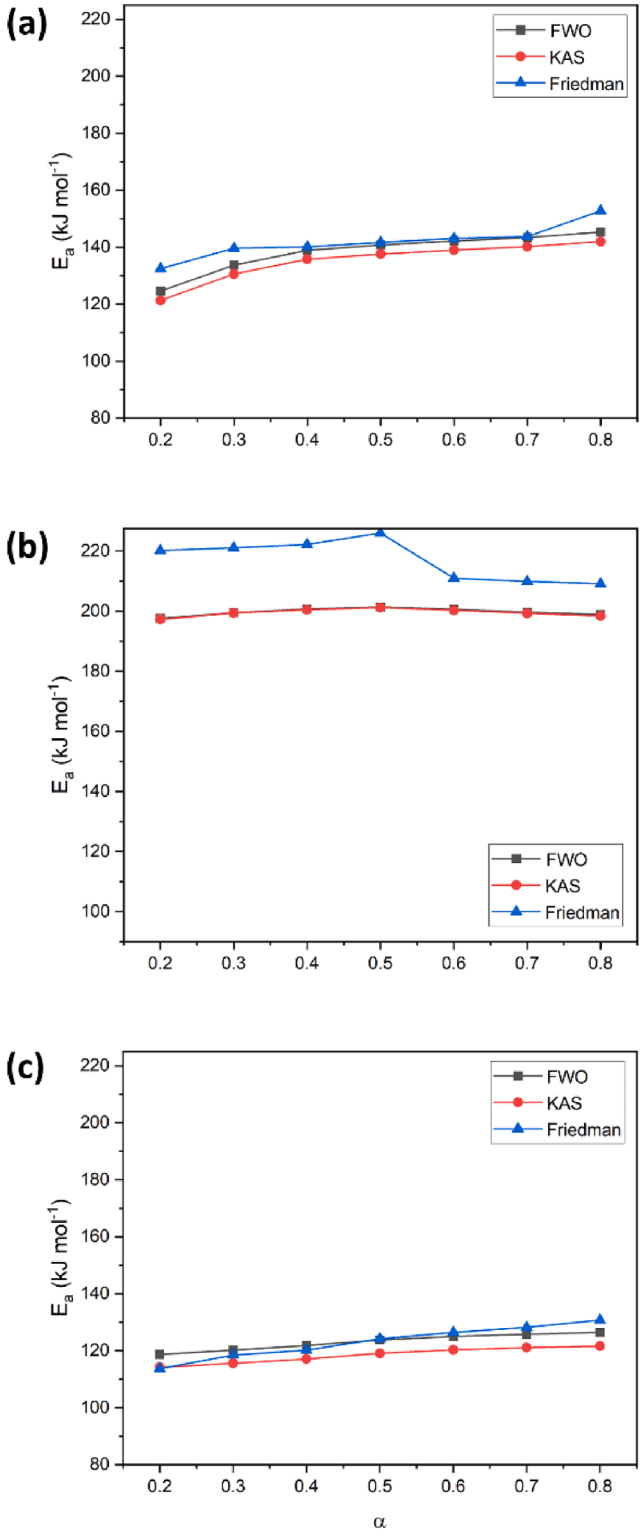

Fig. 4. The activation energy of the pyrolysis process of (a) RSPR, (b) PLA, and (c) RSPR/PLA composite at different conversion rates.

model for RSPR/PLA composite. It was crucial to determine the reaction model to guide the selection or designation of the pyrolysis reactor [52]. The curves of α versus $P(u)/P(u_{0.5})$ obtained from TGA of the pure PLA and RSPR at 5 ℃ min^{-1}, 10 ℃ min^{-1}, and 20 ℃ min^{-1} are shown in Fig. 5(a and b). The $P(u)/P(u_{0.5})$ curves of the above two specimens were generally similar, which suggested the pyrolysis of the pure PLA and RSPR followed the single kinetic model [53]. Fig. 5(c and d) shows the

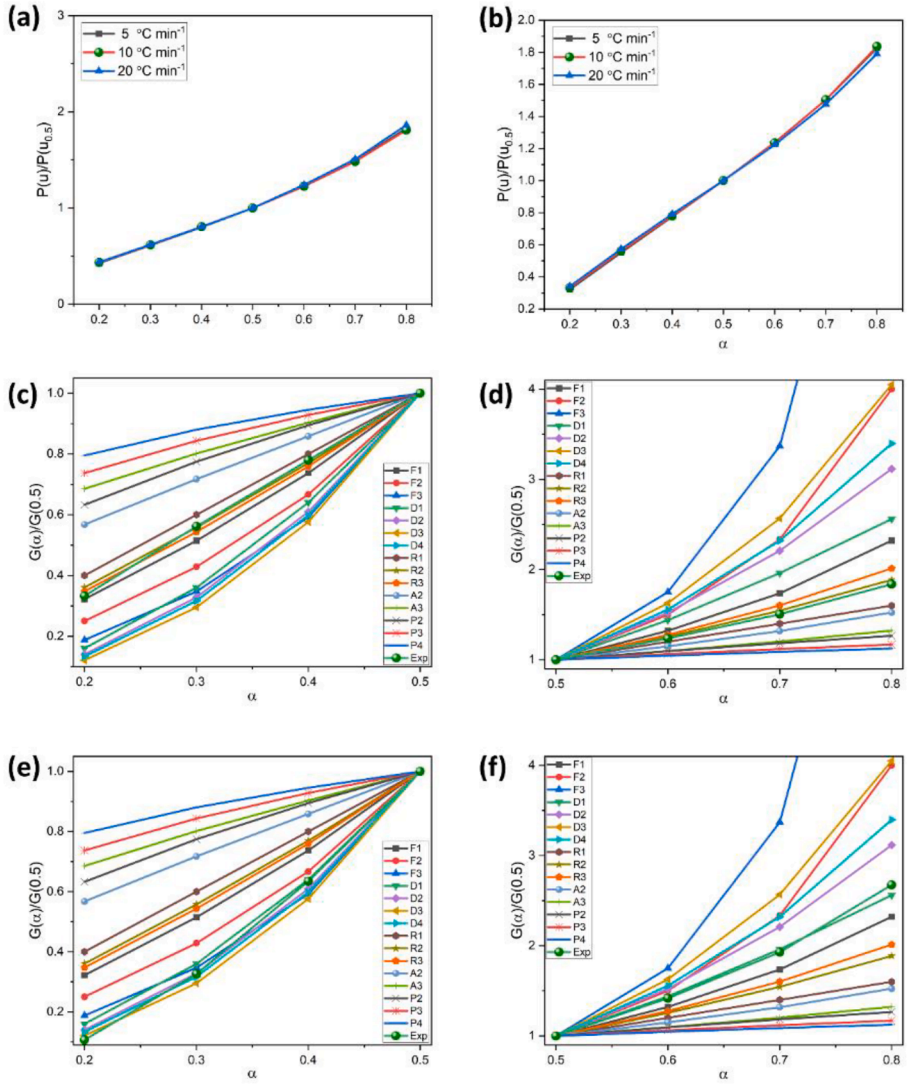

Fig. 5. The curves of α versus P(u)/P($u_{0.5}$) obtained from TG results of (a) PLA; (b) RSPR/PLA composite at 5 ℃ min^{-1}, 10 ℃ min^{-1} and 20 ℃ min^{-1}; the comparison of the experimental and theoretical master plots of PLA (c, d) and RSRP/PLA composite (e, f) at heating rate of 10 ℃ min^{-1}.

comparison of the curves of α versus $G(\alpha)/G(0.5)$ plotted by various theoretical kinetic functions (Table S1) and experimental master-plots $P(u)/P(u_{0.5})$ of PLA at heating rate of 10 ℃ min^{-1}. The experimental master-plots of PLA were consistent with the contracting cylinder model (R2), which coincided with the results in previous research [19]. Similar with most petroleum-based plastics, the pyrolysis mechanism of PLA belongs to the geometrical contraction model[54], which indicates the pyrolysis occurred rapidly on the surface of PLA crystal and the degradation rate was controlled by bounded centre-oriented reaction[55]. As compared to RSPR/PLA composite, the reaction mechanism for the pyrolysis of RSPR/PLA composite can be divided into two parts. There was no matching reaction model can be found in the range of conversation rate from 0.2 to 0.4. In the range of 0.4–0.8, the experimental master-plot curve matched the diffusion model (D1) (Fig. 5(e) and (f)). Therefore, one-dimensional (D1) diffusion model was dominated to the pyrolysis process of RSPR/PLA composite. In addition, D1 model was suggested the conversion rate was proportional to the thickness of the product barrier layer but did not consider the shape factors [56].

3.3.3. *The evaluation of thermodynamic parameters*

The thermodynamic parameters are crucial to optimize the pyrolysis reactor [57]. The thermodynamic parameters calculated by Eq. (9)-Eq. (12) using the different E_a obtained from FWO, KAS and Friedman methods were listed in Table 3. The ΔH refers to the energy consumption of breaking chemical bonds of material and forming new chemical bonds [46]. As can be seen, the ΔH of RSPR/PLA composite were positive, which indicated the pyrolysis of RSPR/PLA composite were endothermic. ΔG represents the whole energy changes of the pyrolysis system for the activated complex formation [19]. So, a lower value of ΔG is more favourable for reaction to take place. The average ΔG of RSPR/PLA composite by FWO, KAS and Friedman methods were 175.7 kJ mol^{-1}, 180.6 kJ mol^{-1} and 175.7 kJ mol^{-1}, respectively. ΔS reflects to the randomness or disorder degree of the pyrolysis system. Typically, the negative value of ΔS illustrates the reactivity of the material was low, which leads to a longer time for the formation of the activated complex, and the activated complex has a higher degree of arrangement [58]. In the pyrolysis process of RSPR/PLA composite, all the ΔS values were negative, inferring the pyrolytic conversion of PLA composite forms an activated complex with a more organized structure than that of the initial material.

4. Conclusion

In this study, to improve the economic feasibility of discarded PLA-based composite disposal, the pyrolysis behaviour and kinetics of RSPR/PLA composite as the model were investigated. The TG-FTIR

Table 3
Thermodynamic parameters of RSPR/PLA composite calculated by FWO, KAS and Friedman method at heating rate of 10 ℃ min^{-1}.

α	A (s^{-1})	ΔH (kJ/mol)	ΔG (kJ/mol)	ΔS (J mol^{-1} K^{-1})	A (s^{-1})	ΔH (kJ/mol)	ΔG (kJ/mol)	ΔS (J mol^{-1} K^{-1})	A (s^{-1})	ΔH (kJ/mol)	ΔG (kJ/mol)	ΔS (J mol^{-1} K^{-1})
	FWO				KAS				Friedman			
0.2	5.16×10^{8}	113.4	170.7	−85.1	2.22×10^{8}	108.9	175.6	−99.1	2.02×10^{8}	108.4	176.1	−100.6
0.3	6.83×10^{8}	114.8	174.1	−88.1	2.89×10^{8}	110.2	178.9	−102.0	4.97×10^{8}	113.1	175.9	−93.3
0.4	9.21×10^{8}	116.4	174.1	−85.7	3.82×10^{8}	111.7	179.0	−100.0	6.83×10^{8}	114.8	175.8	−90.6
0.5	1.34×10^{9}	118.3	176.0	−85.7	5.56×10^{8}	113.6	180.9	−100.0	1.44×10^{9}	118.7	175.6	−84.5
0.6	1.67×10^{9}	119.5	177.0	−85.4	6.96×10^{8}	114.8	181.9	−99.7	2.17×10^{9}	120.9	175.5	−81.1
0.7	1.94×10^{9}	120.2	177.9	−85.7	8.08×10^{8}	115.5	182.8	−100.0	3.04×10^{9}	122.6	175.4	−78.4
0.8	2.17×10^{9}	120.8	179.9	−87.8	$8.87E\times10^{8}$	116.0	184.9	−102.3	4.94×10^{9}	125.2	175.3	−74.4
Average	$\mathbf{1.32\times10^{09}}$	**117.6**	**175.7**	**−86.2**	$\mathbf{5.49\times10^{8}}$	**113.0**	**180.6**	**−100.4**	$\mathbf{1.85\times10^{9}}$	**117.7**	**175.7**	**−86.1**

results demonstrated the presence of RSPR as the reinforcement phase could facilitate the free radical reaction of PLA during the pyrolysis process, leading to the reduction of CO and CO_2 group in the pyrolysis of REPR/PLA composite. Compared with the pyrolysis of the pure PLA (205.5 kJ mol^{-1}) and RSPR (136.5 kJ mol^{-1}) in control groups, lower activation energy (E_a) was realized in the group of RSPR/PLA composite (121.5 kJ mol^{-1}), confirming the synergistic interactions between RSPR and PLA in the composite material. Besides, the results of master-plots method show one-dimensional (D1) diffusion model dominated the RSPR/PLA composite pyrolysis process. This study provides valuable insights regarding the thermal behaviours and kinetics of the pyrolysis of lignocellulose/PLA composites, which not only enhanced the economic value of discarded lignocellulose/PLA composites but also provided a solution for the potential waste lignocellulose/PLA composites pollution.

CRediT authorship contribution statement

Bo Chen: Writing – review & editing, Writing – original draft, Visualization, Methodology, Funding acquisition, Data curation, Conceptualization. **Sen Ma:** Methodology, Investigation. **Sachin Kumar:** . **Zhitong Yao:** Writing – review & editing. **Wanqi Feng:** Software, Resources. **Jianbo Zhao:** Methodology, Investigation. **Xu Zhang:** Resources. **Di Cai:** Writing – review & editing, Supervision, Conceptualization. **Hui Cao:** Supervision, Funding acquisition. **Ian Watson:** Supervision.

Declaration of competing interest

The authors declare that they have no known competing financial interests or personal relationships that could have appeared to influence the work reported in this paper.

Acknowledgements

This work was funded by the Bingtuan Science and Technology Program (Grant No. 2022DB025), Engineering and Physical Sciences Research Council (EPSRC) (Grant No. EP/M01343X/1), and China Scholarship Council, China (Grant No. 201906880041).

Appendix A. Supplementary data

Supplementary data to this article can be found online at https://doi.org/10.1016/j.crcon.2024.100226.

References

[1] S. Ramanadha reddy, Dr.N. Venkatachalapathi, A review on characteristic variation in PLA material with a combination of various nano composites, Mater Today Proc (2023). https://doi.org/10.1016/J.MATPR.2023.04.616.
[2] K.J. Jem, B. Tan, The development and challenges of poly (lactic acid) and poly (glycolic acid), Advanced Industrial and Engineering Polymer Research 3 (2020), https://doi.org/10.1016/j.aiepr.2020.01.002.
[3] X. Hu, D. Ma, G. Zhang, M. Ling, Q. Hu, K. Liang, J. Lu, Y. Zheng, Microwave-assisted pyrolysis of waste plastics for their resource reuse: A technical review, Carbon Resources Conversion 6 (2023), https://doi.org/10.1016/j.crcon.2023.03.002.
[4] C. Sun, W. Li, X. Chen, C. Li, H. Tan, Y. Zhang, Synergistic interactions for saving energy and promoting the co-pyrolysis of polylactic acid and wood flour, Renew Energy 171 (2021), https://doi.org/10.1016/j.renene.2021.02.099.
[5] T.A. Swetha, V. Ananthi, A. Bora, N. Sengottuvelan, K. Ponnuchamy, G. Muthusamy, A. Arun, A review on biodegradable polylactic acid (PLA) production from fermentative food waste - Its applications and degradation, Int J Biol Macromol 234 (2023), https://doi.org/10.1016/j.ijbiomac.2023.123703.
[6] S. Ma, X. Yang, Z. Guo, X. Zhang, T. Tan, Co-production of additive manufacturing composites with solid residue from enzymatic hydrolysis of reed, J Clean Prod 249 (2020), https://doi.org/10.1016/j.jclepro.2019.119421.
[7] S. Kumar, Y.S. Varadarajan, M.S. Shamprasad, Three-body abrasive wear behavior of rice straw fibers reinforced PLA composites, Mater Today Proc (2023), https://doi.org/10.1016/J.MATPR.2023.05.009.
[8] M.H.M. Hamdan, J.P. Siregar, M.R.M. Rejab, D. Bachtiar, J. Jamiluddin, C. Tezara, Effect of Maleated Anhydride on Mechanical Properties of Rice Husk Filler Reinforced PLA Matrix Polymer Composite, International Journal of Precision Engineering and Manufacturing - Green Technology 6 (2019), https://doi.org/10.1007/s40684-019-00017-4.
[9] S. Kumar, M.S. Shamprasad, Y.S. Varadarajan, M.A. Sangamesha, Coconut coir fiber reinforced polypropylene composites: Investigation on fracture toughness and mechanical properties, Mater Today Proc (2021), https://doi.org/10.1016/j.matpr.2021.01.402.
[10] O. Gordobil, R. Delucis, I. Egüés, J. Labidi, Kraft lignin as filler in PLA to improve ductility and thermal properties, Ind Crops Prod 72 (2015), https://doi.org/10.1016/j.indcrop.2015.01.055.
[11] A.A. Thompson, M.B. Samuelson, I. Kadoma, E. Soto-Cantu, R. Drijber, S. E. Wortman, Degradation Rate of Bio-based Agricultural Mulch is Influenced by Mulch Composition and Biostimulant Application, J Polym Environ 27 (2019), https://doi.org/10.1007/s10924-019-01371-9.
[12] C. Li, Q. Liu, W. Gong, Z. Zhou, Z. Yao, X. Meng, Study on the atomic scale of thermal and thermo-oxidative degradation of polylactic acid via reactive molecular dynamics simulation, Thermochim Acta 709 (2022), https://doi.org/10.1016/j.tca.2021.179144.
[13] C. Sun, C. Li, H. Tan, Y. Zhang, Synergistic effects of wood fiber and polylactic acid during co-pyrolysis using TG-FTIR-MS and Py-GC/MS, Energy Convers Manag 202 (2019) 112212, https://doi.org/10.1016/J.ENCONMAN.2019.112212.
[14] S. Wang, Y. Sun, R. Shan, J. Gu, T. Huhe, X. Ling, H. Yuan, Y. Chen, Polypropylene pyrolysis and steam reforming over Fe-based catalyst supported on activated carbon for the production of hydrogen-rich syngas, Carbon Resources Conversion 6 (2023), https://doi.org/10.1016/j.crcon.2023.02.004.
[15] H. Nishida, T. Mori, S. Hoshihara, Y. Fan, Y. Shirai, T. Endo, Effect of tin on poly(L-lactic acid) pyrolysis, Polym Degrad Stab 81 (2003), https://doi.org/10.1016/S0141-3910(03)00152-6.
[16] F. Zhang, Y. Sun, J. Li, H. Su, Z. Zhu, B. Yan, Z. Cheng, G. Chen, Pyrolysis of 3D printed polylactic acid waste: A kinetic study via TG-FTIR/GC-MS analysis, J Anal Appl Pyrolysis 166 (2022), https://doi.org/10.1016/j.jaap.2022.105631.
[17] I.C. McNeill, H.A. Leiper, Degradation studies of some polyesters and polycarbonates-2. Polylactide: Degradation under isothermal conditions, thermal degradation mechanism and photolysis of the polymer, Polym Degrad Stab 11 (1985), https://doi.org/10.1016/0141-3910(85)90035-7.
[18] G. Sivalingam, G. Madras, Thermal degradation of binary physical mixtures and copolymers of poly(ε-caprolactone), poly(D, L-lactide), poly(glycolide), Polym Degrad Stab 84 (2004), https://doi.org/10.1016/j.polymdegradstab.2003.12.008.
[19] C. Sun, X. Chen, D. Zheng, W. Yao, H. Tan, Y. Zhang, S. Liu, Exploring the synergetic effects of the major components of biomass additives in the pyrolysis of polylactic acid, Green Chemistry 23 (2021), https://doi.org/10.1039/d1gc03002g.
[20] X. Gou, X. Zhao, S. Singh, D. Qiao, Tri-pyrolysis: A thermo-kinetic characterisation of polyethylene, cornstalk, and anthracite coal using TGA-FTIR analysis, Fuel 252 (2019), https://doi.org/10.1016/j.fuel.2019.03.143.
[21] K.W. Chew, S.R. Chia, W.Y. Chia, W.Y. Cheah, H.S.H. Munawaroh, W.J. Ong, Abatement of hazardous materials and biomass waste via pyrolysis and co-pyrolysis for environmental sustainability and circular economy, Environmental Pollution 278 (2021), https://doi.org/10.1016/j.envpol.2021.116836.

[22] J. Liu, X. Jiang, H. Cai, F. Gao, Study of Combustion Characteristics and Kinetics of Agriculture Briquette Using Thermogravimetric Analysis, ACS Omega 6 (2021), https://doi.org/10.1021/acsomega.1c01249.
[23] J. Liu, L. Luo, Z. Zhang, Y. Hu, F. Wang, X. Li, K. Tang, A combined kinetic study on the pyrolysis of chrome shavings by thermogravimetry, Carbon Resources Conversion 3 (2020), https://doi.org/10.1016/j.crcon.2020.11.003.
[24] S. Patnaik, A.K. Panda, S. Kumar, Thermal degradation of corn starch based biodegradable plastic plates and determination of kinetic parameters by isoconversional methods using thermogravimetric analyzer, Journal of the Energy Institute 93 (2020), https://doi.org/10.1016/j.joei.2020.01.007.
[25] V. Balasundram, N. Ibrahim, R.M. Kasmani, M.K. Abd Hamid, R. Isha, H. Hasbullah, R.R. Ali, Thermogravimetric catalytic pyrolysis and kinetic studies of coconut copra and rice husk for possible maximum production of pyrolysis oil, J Clean Prod 167 (2017) 218–228. <Go to ISI>://WOS:000413128100021.
[26] H.E. Kissinger, Reaction Kinetics in Differential Thermal Analysis, Anal Chem 29 (1957) 1702–1706, https://doi.org/10.1021/ac60131a045.
[27] B. Chen, Z. Yao, C. Zhang, S. Cheng, M. Zhu, Y. Wang, Y. Wu, H. Cao, I. Watson, D. Cai, Catalytic co-pyrolysis of cellulosic ethanol–processing residue with high-density polyethylene over biomass bottom ash catalyst, Biomass Convers Biorefin (2023), https://doi.org/10.1007/s13399-023-03915-5.
[28] V.A. Yiga, M. Lubwama, P.W. Olupot, Pyrolysis, kinetics and thermodynamic analyses of rice husks/clay fiber-reinforced polylactic acid composites using thermogravimetric analysis, J Therm Anal Calorim 148 (2023), https://doi.org/10.1007/s10973-022-11927-y.
[29] C. Zhang, H. Chen, N. An, C. Su, M. Lv, S. Pang, X. Wang, D. Cai, P. Qin, Impact of corn stover harvest time and cultivars on acetone-butanol-ethanol production, Ind Crops Prod 139 (2019), https://doi.org/10.1016/j.indcrop.2019.111500.
[30] A. Sluiter, B. Hames, R. Ruiz, C. Scarlata, J. Sluiter, D. Templeton, D. Crocker, Determination of structural carbohydrates and lignin in biomass, Laboratory Analytical Procedure 1617 (2008) 1–16.
[31] M.J. Starink, The determination of activation energy from linear heating rate experiments: a comparison of the accuracy of isoconversion methods, Thermochim Acta 404 (2003) 163–176. <Go to ISI>://WOS:000185448300020.
[32] C.D. Doyle, Estimating isothermal life from thermogravimetric data, J Appl Polym Sci 6 (1962) 639–642, https://doi.org/10.1002/app.1962.070062406.
[33] H.L. Friedman, Kinetics of thermal degradation of char-forming plastics from thermogravimetry. Application to a phenolic plastic, Journal of Polymer Science Part c: Polymer Symposia 6 (1964), https://doi.org/10.1002/polc.5070060121.
[34] F.J. Gotor, M. José, J. Criado, N.K. Malek, Kinetic analysis of solid-state reactions: The universality of master plots for analyzing isothermal and nonisothermal experiments, Journal of Physical Chemistry A 104 (2000), https://doi.org/10.1021/jp0022205.
[35] I. Ali, Misuse of pre-exponential factor in the kinetic and thermodynamic studies using thermogravimetric analysis and its implications, Bioresour Technol Rep 2 (2018), https://doi.org/10.1016/j.biteb.2018.04.011.
[36] I. Ali, R.C. Seyfeli, M.H. Tahir, S. Ceylan, Pyrolytic conversion of waste hemp: Kinetics, product characterization, and boosted regression tree modeling, J Anal Appl Pyrolysis 175 (2023), https://doi.org/10.1016/j.jaap.2023.106165.
[37] B. Chen, D. Cai, Z.F. Luo, C.J. Chen, C.W. Zhang, P.Y. Qin, H. Cao, T.W. Tan, Corncob residual reinforced polyethylene composites considering the biorefinery process and the enhancement of performance, J Clean Prod 198 (2018) 452–462. <Go to ISI>://WOS:000442973100039.
[38] Z. Ma, D. Chen, J. Gu, B. Bao, Q. Zhang, Determination of pyrolysis characteristics and kinetics of palm kernel shell using TGA-FTIR and model-free integral methods, Energy Convers Manag 89 (2015), https://doi.org/10.1016/j.enconman.2014.09.074.
[39] H. Cai, J. Liu, W. Xie, J. Kuo, M. Buyukada, F. Evrendilek, Pyrolytic kinetics, reaction mechanisms and products of waste tea via TG-FTIR and Py-GC/MS, Energy Convers Manag 184 (2019) 436–447, https://doi.org/10.1016/j.enconman.2019.01.031.
[40] K. Setswalo, O.P. Oladijo, M. Namoshe, E.T. Akinlabi, M.R. Sanjay, The mechanical properties of alkali and laccase treated pterocarpus angolensis (mukwa)-polylactic acid (PLA) composites, Int J Biol Macromol 217 (2022) 398–406, https://doi.org/10.1016/j.ijbiomac.2022.07.075.
[41] J. Ordonez-Loza, F. Chejne, A.G.A. Jameel, S. Telalovic, A.A. Arrieta, S.M. Sarathy, An investigation into the pyrolysis and oxidation of bio-oil from sugarcane bagasse: Kinetics and evolved gases using TGA-FTIR, J Environ Chem Eng 9 (2021), https://doi.org/10.1016/j.jece.2021.106144.
[42] M.H. Tahir, I. Ali, E.Y. Kaya, S. Ceylan, Thermal conversion of waste furniture board under pyrolytic conditions: Kinetic analysis and product characterization, Fuel 348 (2023), https://doi.org/10.1016/j.fuel.2023.128638.
[43] S. Lv, Y. Zhang, H. Tan, Thermal and thermo-oxidative degradation kinetics and characteristics of poly (lactic acid) and its composites, Waste Management 87 (2019), https://doi.org/10.1016/j.wasman.2019.02.027.
[44] G.D. Mumbach, J.L.F. Alves, J.C.G. da Silva, M. Di Domenico, C. Marangoni, R.A. F. Machado, A. Bolzan, Investigation on prospective bioenergy from pyrolysis of butia seed waste using TGA-FTIR: Assessment of kinetic triplet, thermodynamic parameters and evolved volatiles, Renew Energy 191 (2022), https://doi.org/10.1016/j.renene.2022.03.159.
[45] G. Özsin, A.E. Pütün, TGA/MS/FT-IR study for kinetic evaluation and evolved gas analysis of a biomass/PVC co-pyrolysis process, Energy Convers Manag 182 (2019), https://doi.org/10.1016/j.enconman.2018.12.060.
[46] Y. Liu, Y. Song, J. Fu, W. Ao, A. Ali Siyal, C. Zhou, C. Liu, M. Yu, Y. Zhang, J. Dai, X. Bi, Co-pyrolysis of sewage sludge and lignocellulosic biomass: Synergistic effects on products characteristics and kinetics, Energy Convers Manag 268 (2022) 116061, https://doi.org/10.1016/J.ENCONMAN.2022.116061.
[47] D.J. Nowakowski, J.M. Jones, R.M.D. Brydson, A.B. Ross, Potassium catalysis in the pyrolysis behaviour of short rotation willow coppice, Fuel 86 (2007) 2389–2402, https://doi.org/10.1016/J.FUEL.2007.01.026.
[48] L. Gašparoviè, J. Labovský, J. Markoš, L. Jelemenský, Calculation of kinetic parameters of the thermal decomposition of wood by distributed activation energy model (DAEM), Chem Biochem Eng Q 26 (2012).
[49] A.A.D. Maia, L.C. de Morais, Kinetic parameters of red pepper waste as biomass to solid biofuel, Bioresour Technol 204 (2016), https://doi.org/10.1016/j.biortech.2015.12.055.
[50] M. Musioł, W. Sikorska, G. Adamus, H. Janeczek, J. Richert, R. Malinowski, G. Jiang, M. Kowalczuk, Forensic engineering of advanced polymeric materials. Part III - Biodegradation of thermoformed rigid PLA packaging under industrial composting conditions, Waste Management 52 (2016), https://doi.org/10.1016/j.wasman.2016.04.016.
[51] Z. Wang, G. Liu, D. Shen, C. Wu, S. Gu, Co-pyrolysis of lignin and polyethylene with the addition of transition metals - Part I: Thermal behavior and kinetics analysis, Journal of the Energy Institute 93 (2020), https://doi.org/10.1016/j.joei.2019.03.003.
[52] G. Gözke, Kinetic and thermodynamic analyses based on thermogravimetric pyrolysis of watermelon seed by isoconversional and master plots methods, Renew, Energy 201 (2022) 916–927, https://doi.org/10.1016/J.RENENE.2022.10.100.
[53] Y. Qu, A. Li, D. Wang, L. Zhang, G. Ji, Kinetic study of the effect of in-situ mineral solids on pyrolysis process of oil sludge, Chemical Engineering Journal 374 (2019), https://doi.org/10.1016/j.cej.2019.05.183.
[54] J.T. Carstensen, Stability of solids and solid dosage forms, J Pharm Sci 63 (1974), https://doi.org/10.1002/jps.2600630103.
[55] A. Khawam, D.R. Flanagan, Solid-state kinetic models: Basics and mathematical fundamentals, Journal of Physical Chemistry B 110 (2006), https://doi.org/10.1021/jp062746a.
[56] Q. He, L. Ding, Y. Gong, W. Li, J. Wei, G. Yu, Effect of torrefaction on pinewood pyrolysis kinetics and thermal behavior using thermogravimetric analysis, Bioresour Technol 280 (2019), https://doi.org/10.1016/j.biortech.2019.01.138.
[57] B.H. Lee, V. Thieu Trinh, H. Bin Moon, J.H. Lee, H.T. Kim, J.W. Lee, C.H. Jeon, Physicochemical properties and pyrolysis behavior of petcoke with artificial neural network modeling, Fuel 331 (2023), https://doi.org/10.1016/j.fuel.2022.125735.
[58] Y. Xu, B. Chen, Investigation of thermodynamic parameters in the pyrolysis conversion of biomass and manure to biochars using thermogravimetric analysis, Bioresour Technol 146 (2013), https://doi.org/10.1016/j.biortech.2013.07.086.